Operational Modal Analysis of the Space Launch System Mobile Launcher on the Crawler Transporter ISVV-010 Rollout

James C. Akers[1] and Joel W. Sills Jr.[2]

[1] NASA Glenn Research Center
21000 Brookpark Road
Cleveland, Ohio 44135

[2] NASA Johnson Space Center
2101 NASA Parkway
Houston, TX 77058

ABSTRACT
NASA is developing an expendable heavy lift launch vehicle capability, the Space Launch System, to support lunar and deep space exploration. To support this capability, an updated ground infrastructure is required including modifying an existing Mobile Launcher system. The Mobile Launcher is a very large heavy beam/truss steel structure designed to support the Space Launch System during its buildup and integration in the Vehicle Assembly Building, transportation between the Vehicle Assembly Building and launch pad 39B by the Crawler Transporter, and provides the launch platform at the launch pad. As part of the Verification and Validation of the Mobile Launcher and Crawler Transporter, two rollouts of the Mobile Launcher transported by the Crawler Transporter, Integrated System Verification and Validation (ISVV) 005 and 010, have been performed to demonstrate the Crawler Transporter's ability to transport the Mobile Launcher. ISVV-005 occurred in September 2018 and ISVV-010 occurred in late June 2019. ISVV-005 and ISVV-010 also provided the opportunity to gather data that can be used identify the Mobile Launcher on the Crawler Transporter rollout modal characteristics and refine the estimates of the Artemis I integrated launch vehicle rollout forcing functions. While the rollout environment has historically produced relatively small launch vehicle structural loads for the Saturn/Apollo and Space Shuttle programs in comparison to launch and ascent loads, these relatively small structural loads are inputs to structural fatigue analyses. The same holds true for the Space Launch System. Because the rollout forces acting on the Mobile Launcher and the Crawler Transporter are not directly measurable, Operational Modal Analysis techniques, instead of traditional Experimental Modal Analysis techniques, provide an empirical means to identify the Mobile Launcher on the Crawler Transporter rollout modal characteristics. The ISVV-010 rollout modal characteristics provide important supplemental modal information, which along with the Mobile Launcher modal test that was performed in June 2019 immediately prior to ISVV-010 rollout, combine to reduce uncertainty in the test correlated Mobile Launcher on the Crawler Transporter finite element model. A well test correlated finite element model will play a key role in the Building Block approach the Space Launch System program has implemented as part of its certification process for the Artemis I flight and in refining the Artemis I rollout forcing functions. At the time of the ISVV-005 rollout in September 2018, the Mobile Launcher was still undergoing construction, and therefore its modal characteristics are not directly comparable to those of the Mobile Launcher during the June 2019 Mobile Launcher modal test and subsequent ISVV-010 rollout. Hence the ISVV-005 rollout modal characteristics will not be looked at in this paper. This paper will briefly describe the Mobile Launcher and Crawler Transporter physical characteristics, ISVV-010 rollout data collection, the challenges in implementing Operational Modal Analysis techniques due in part to the Crawler Transporter harmonics, and how these challenges were overcome to obtain the ISVV-010 Mobile Launcher on the Crawler Transporter rollout modal characteristics.

Keywords: Apollo, Artemis I, Building Block Approach, Crawler Transporter, Experimental Modal Analysis, Finite Element Model, Harmonics, ISVV-005, ISVV-010, Launch Pad 39B, Mobile Launcher, Modal Characteristics, NASA, Operational Modal Analysis, Rollout, Rollout Forcing Functions, Saturn, Space Launch System, Space Shuttle, Vehicle Assembly Building, Verification and Validation

BACKGROUND

The National Aeronautics and Space Administration (NASA) is developing the expendable heavy lift launch vehicle, the Space Launch System (SLS), to support lunar and deep space exploration [1, 2]. The Mobile Launcher (ML) is a very large and very heavy open beam/truss steel structure designed to support SLS during its buildup and integration in the Vehicle Assembly Building (VAB), transportation from the VAB out to the launch pad, and provides the launch platform at the launch pad. The ML consists of a Tower and Deck structures. The ML Tower weighs 4 million pounds, is 355 feet tall, and the upper levels are 40 square feet with floors every 20 feet for personnel access. The ML Deck is a two-story structure 25 feet high, 165 feet long, 135 feet wide, weighing 6 million pounds. ML weighs approximately 10.6 million pounds and is over 380 feet tall [3]. The ML Deck supports the SLS at eight attachment points located at the bottom of its two boosters, which connect to the ML Vehicle Support Posts (VSP). The ML Tower provides lateral support to the integrated SLS launch vehicle via the Vehicle Stabilization System (VSS) and supports the fuel, power, and data umbilicals running to SLS and MPCV. The ML Tower also provides crew access to the Orion Multi-Purpose Crew Vehicle (MPCV) Crew Module (CM) via the Crew Access Arm (CAA). Figure 1 shows the Artemis I integrated vehicle on the ML [4]. For the Artemis I rollout, all of the umbilicals and Vehicle Stabilizer System (VSS) will be connected, but the CAA will be retracted and rotated to the side of the ML Tower.

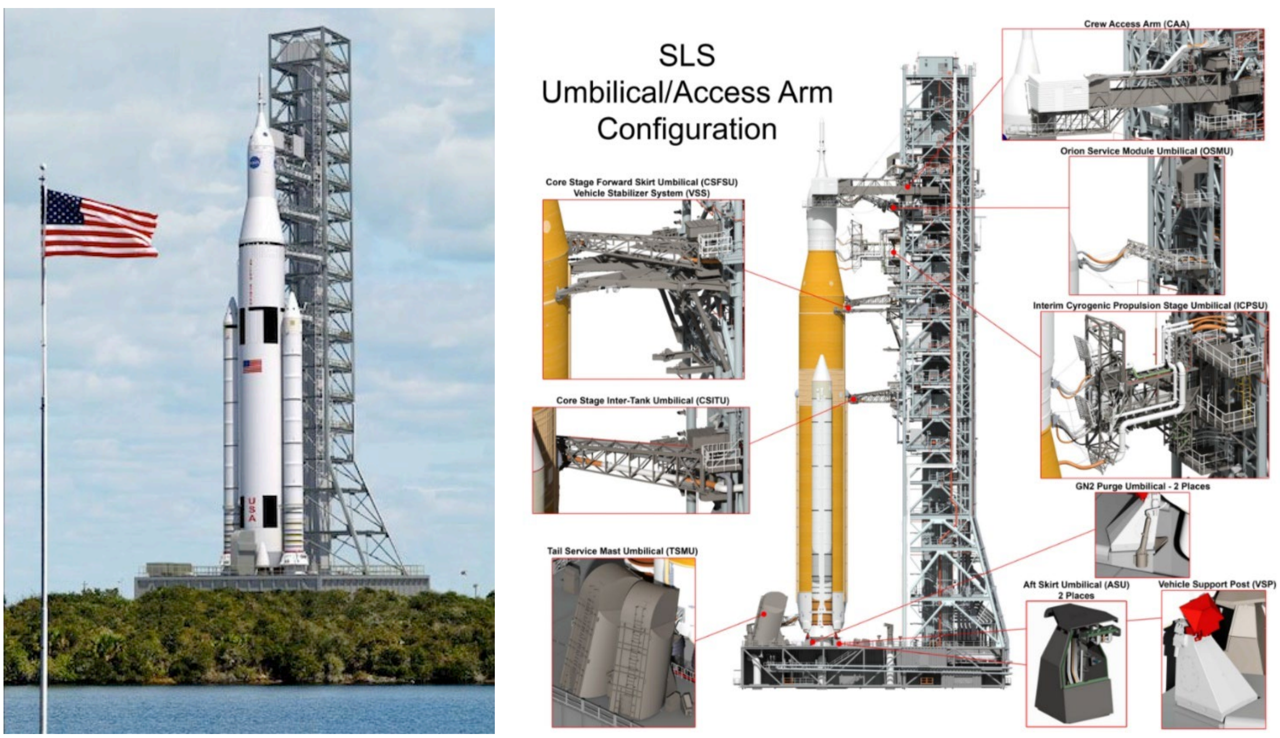

Figure 1. SLS on Mobile Launcher at Launch Pad (left) and Umbilicals (right), (from http://NASASpaceFlight.com).

The Crawler Transporter (CT) performs all lifting and transport operations of both the rollout of the ML with the SLS integrated vehicle from the VAB to Launch Pad 39B and move operations of the ML from the pad after launch. CT-2 is a recently upgraded version of one of the original CT's used for the Apollo and Space Shuttle programs [5 -7] with their design based upon heavy mining machinery. These upgrades allow the CT-2 to carry the heavier loading imposed by the integrated SLS launch vehicle and ML. CT-2 is the size of a baseball infield, with a top speed of 1 mph loaded and 2 mph unloaded. CT-2 weights 6.3 million pounds total, height of between 20 feet and 26 feet depending on its jacking level. Jacking, Equalization and Leveling (JEL) of the ML/SLS is performed by the JEL hydraulic system. Four hydraulic cylinders at each corner are pressurized by redundant pumps and provide for lifting and leveling control of the stack. The JEL's keep the stack level while negotiating the 5% incline to the launch pad. During the ISVV-010 rollout the CT JEL's supported a total weight of 12.8 million pounds, 10.6 million pound ML and 2.2 million pound CT Chassis. The CT maximum load capacity is 18 million pounds. The CT provides vertical support for the ML at four (4) pickup points. Lateral mechanical constraints for the ML is provided at three of the four pickup points to minimize ML-to-CT support constraint stresses. Figure 2 is an aerial view of the CT-2 showing the four pickup points and the lateral mechanical constraints (yellow arrows) at each pickup point. These lateral mechanical constraints (yellow arrows) at each pickup point are designed to provide a lateral kinematic connection between the ML and CT so that ML does not impart static lateral loads into the CT and vice versa. Because of this Corner B has no lateral mechanical constraints.

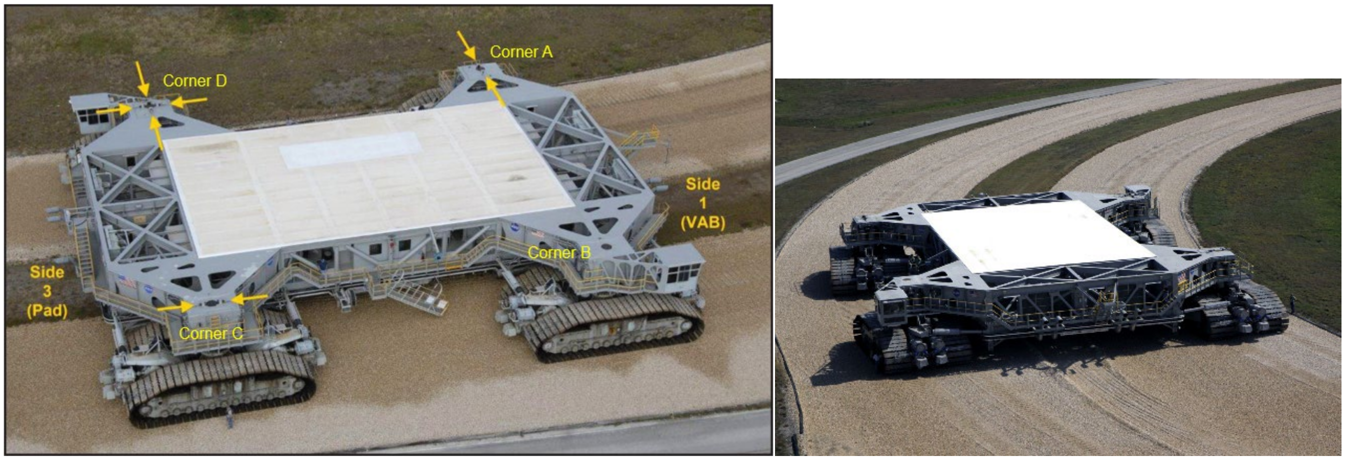

Figure 2. Aerial View of CT-2 Showing Pickup Points [5].

The CT has four trucks, each having two tracks. Each track has 57 shoes with each shoe weighing 2,100 lb. Each track is driven by two 375 hp electric motors (four per truck) that are powered by four 1,000 kW DC generators that in turn are powered by two Alco 16 cylinder diesel engines. While the CT's internal drive train gearing does produce harmonic excitations, the most significant harmonic excitations are generated by the truck tracks and rollers [8]. One set of dominant harmonics is due to the initial slap of the track shoes making contact with the ground, referred to as the shoe slapping harmonics, which are a function of CT speed and shoe spacing. Another set of dominant harmonics is due to the track shoes passing underneath the 11 support rollers of each track, referred to as the roller crossing harmonics, which are also a function of the CT speed and the spacing between the support rollers. Figure 3 shows the CT truck tracks and Figure 4 shows the relationship between these harmonics and the ML on CT fundamental modes. Note that these harmonics are dispersed within the frequency range of these fundamental modes. Although the harmonic frequencies of these two sets of harmonics remain relatively constant for a constant CT speed, the continuous variations in the amplitudes and relative phasing between these harmonics of each track make it very difficult to model analytically and challenging to remove.

Figure 3. CT during ISVV-010 Rollout June 2019 (left) and Rollout Conducted September 2019 (right).

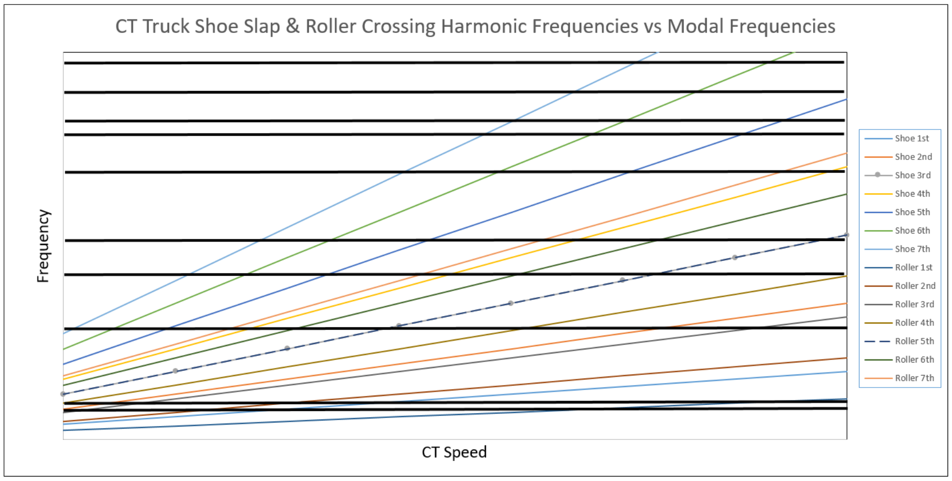

Figure 4. CT Truck Track Shoe and Roller First Seven Harmonics vs ML on CT Fundamental Modal Frequencies.

The ML underwent a modal survey inside the VAB that was completed on June 27, 2019 [9, 10]. The Integrated System Verification and Validation 010 (ISVV-010) rollout occurred immediately afterwards, with the rollout from the VAB beginning around midnight of June 28 and arriving at Launch Pad 39B gate just before 9:00 am. A rollout from the VAB out to Launch Pad 39B takes approximately 8 hours. Figure 5 shows the ML on CT during the ISVV-010 roll out of the VAB. Figure 6 shows the ML on CT after arriving at Launch Pad 39 B the following day June 29. Figure 7 shows the ML on CT during the ISVV-005 rollout in September 2018, which shows the 4.2 mile trek from the VAB to Launch Pad 39B.

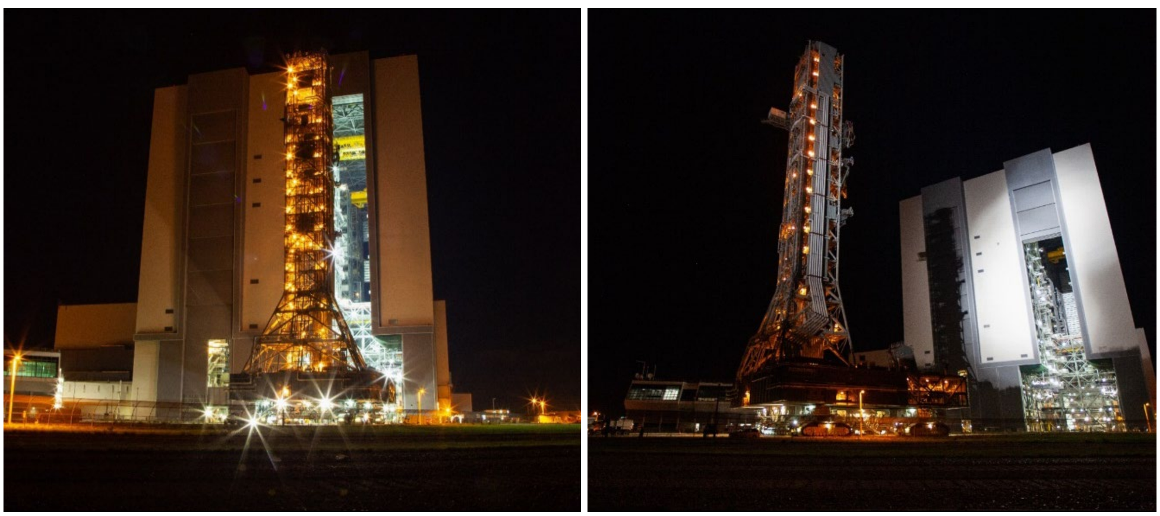

Figure 5. ISVV-010 Rollout, ML on CT Leaving VAB at Midnight June 28.

Figure 6. ML on CT at Launch Pad June 29, 2019.

Figure 7. ISVV-005 Rollout September 2018.

As part of the risk reduction process, the Space Launch System (SLS) program has adopted a building block approach, which a well test correlated ML FEM, correlated to both the ML modal test and ISVV-010 rollout is a key element [11]. Understanding the ML structural dynamic properties are of paramount importance in accurately predicting rollout forcing functions and predicting loads on SLS while at the launch pad that include separation dynamics during liftoff. The ML will also serve as the dynamic modal test fixture for the Integrated Modal Test (IMT) of the Artemis I integrated vehicle [9]. However, during both the ML Only modal test and the ISVV-005 and ISVV-010 rollouts, the ML Deck was not mass loaded like it will be when supporting SLS, and therefore residual uncertainty may exist in the ML Deck portion test correlated ML FEM. Subsequent testing has been baselined by the programs (i.e., Space Launch System, Exploration Ground System, etc.) to gather supplemental ML Deck stiffness data to help to reduce this residual uncertainty.

SPACE SHUTTLE MOBILE LAUNCH PLATFORM AND PARTIAL STACK ROLLOUT

Prior to using OMA techniques on the ISVV-010 Rollout analysis, OMA techniques were used on the 2003 Shuttle-Era Partial Stack rollout data, 2005 Shuttle-era CT rollout data, 2005 Shuttle-Era CT transporting the Mobile Launch Platform (MLP) [12 - 14] rollout data. This was done to gain insights into the Shuttle-era CT structural dynamics in its unloaded and loaded configurations and gain confidence using OMA techniques. Figure 8 shows the Shuttle-era CT transporting the Space Shuttle on the MLP and the Partial Stack rollout configuration. Figure 9 shows the Shuttle-era CT transporting the MLP. MLP did not have a launch tower structure like the current ML.

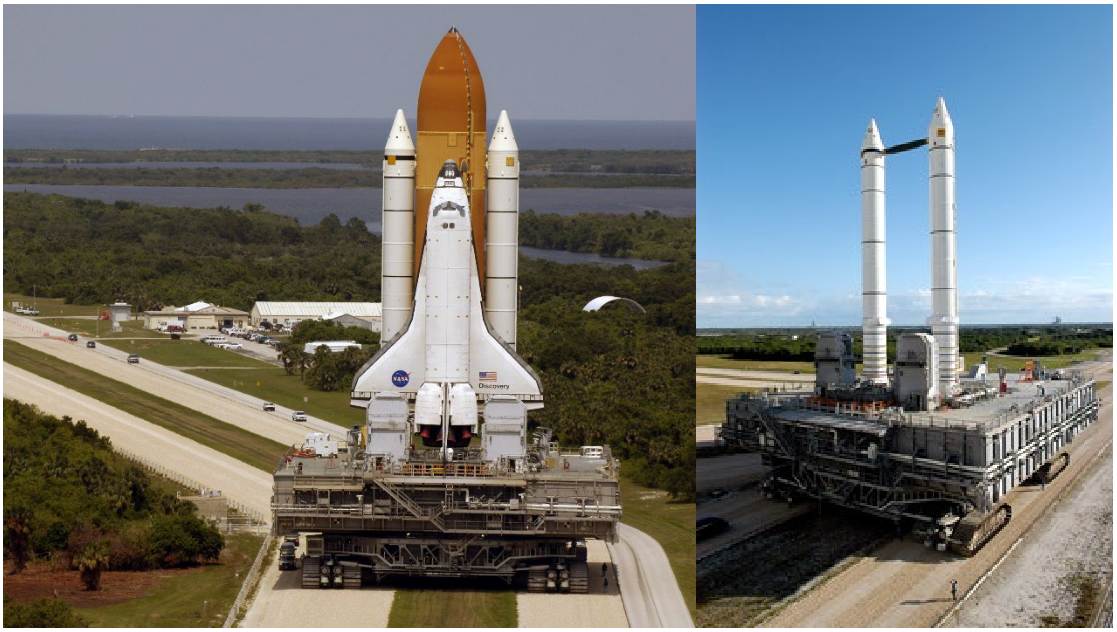

Figure 8. Shuttle-Era CT Transporting Space Shuttle on the MLP (left), Partial Stack Rollout (right).

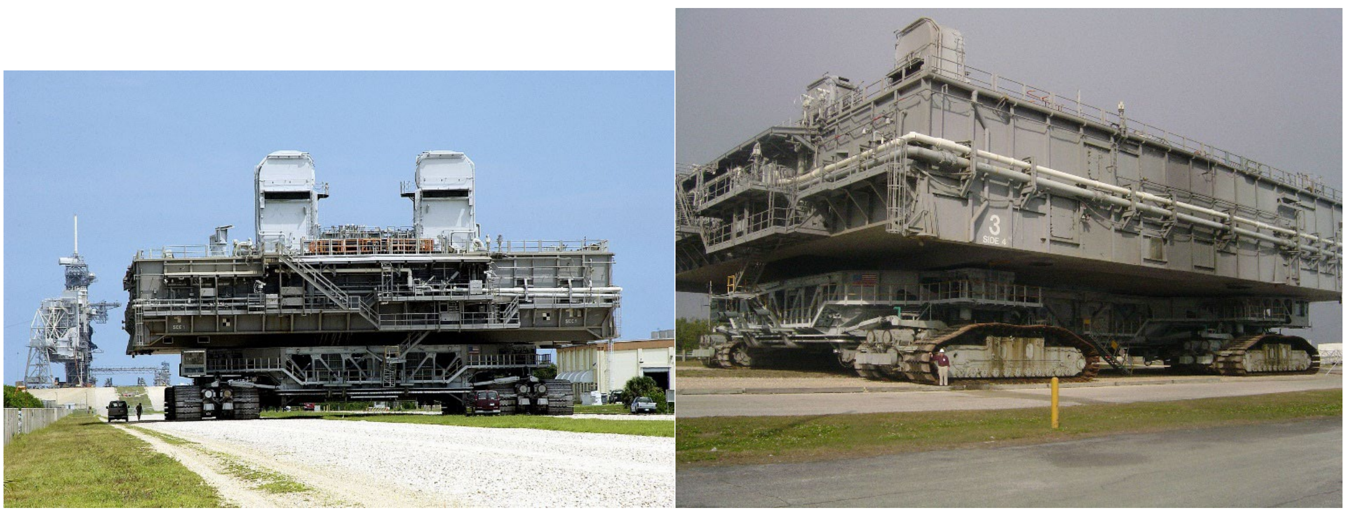

Figure 9. Shuttle-Era CT Transporting MLP.

The Space Shuttle full-stack rollout configuration consisted of an Orbiter Vehicle (OV) attached to an empty External Tank (ET) that was attached to two fueled Solid Rocket Boosters (SRB's) that in turn attach to the MLP. This Space Shuttle full-stack and MLP weighed approximately 12 million pounds [15]. Video of the Space Shuttle Space Transportation System 107 (STS-107) rollout of the Space Shuttle showed that dynamics of the Shuttle and MLP were excited during rollout and raised concerns that the rollout environment was using up more of the fatigue life of certain Orbiter structural members than expected [8, 15]. To better understand this rollout environment and forcing functions, ideally an instrumented rollout of Space Shuttle would have been performed and recorded. Unfortunately, due to a Space Shuttle not being available until rollout for its next flight, and not wanting to impact the Return-to-Flight schedule, this was not possible. Instead a Partial Stack rollout configuration was used that consisted of two fueled SRB's mounted to the MLP with a crossbeam that emulated the forward attachment of the Space Shuttle's External Tank (ET) connecting the SRB's at their forward attachment fitting. The Partial Stack rollout configuration weighed over 90% the Space Shuttle full-stack rollout configuration, which ensured the CT loading was close to what it would see during an actual Space Shuttle rollout.

The Partial Stack rollout included acceleration response time histories from a total of 35 triaxial accelerometers shown in Figure 10 with 3 on each SRB, 20 on the MLP, 9 on the CT, and the CT speed time history [15 -17]. The Partial Stack rollout data was collected during four 10 minute time periods where the CT was stopped and one 10 minute time period where the CT was traveling at maximum velocity and then came to a stop. Previously OMA techniques had been applied to this rollout where the CT was stopped, in order to avoid the complications of the CT shoe and roller crossing harmonics, and successfully identified modes that were subsequently used to update the MLP and CT FEM's [15 - 17]. OMA time-domain and frequency-domain techniques were able to identify modes that agreed very well in modal frequency and whose mode shapes matched the mode shape descriptions given in [17]. However the time-domain techniques failed to identify the two lowest frequency modes, which were the SRB's rocking in the two lateral directions, even though the Singular Value Decomposition (SVD) of the Spectral Density Matrix (SDM) had two well defined peaks as shown in Figure 10. This could be due to the data sets not having sufficient duration. Because the SRB's were directly connected to the MLP deck, they possessed a significant amount of cantilever mass/inertia, and the ground winds were able to excite them sufficiently, their lateral rocking and vertical motion was able to induce sufficient motion in the MLP and CT to allow OMA techniques to successfully identify modes when the CT was stopped. Because the ML Tower similarly represents a significant amount of cantilever mass/inertia, this work indicated that OMA techniques should be able to be successfully identify fundamental modes from the ISVV-010 rollout data collected during periods when the CT was stopped. Finally this work pointed out the importance of the proper selection of Projection Channels and the need for doing thorough data quality checks to remove spurious data effects such as large excursions and data dropouts prior to applying OMA techniques.

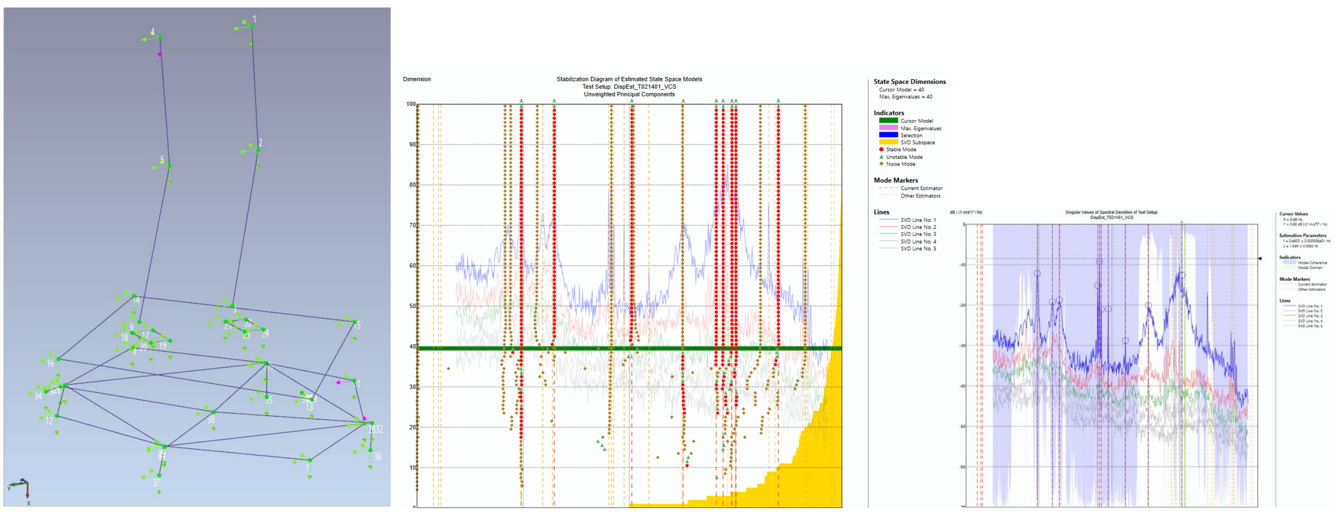

Figure 10. Partial Stack Rollout TDM (left), OMA Time-Domain Technique (center), OMA Frequency-Doman Technique (right).

The 2005 Shuttle-era CT rollout data and the 2005 Shuttle-Era CT transporting the MLP rollout data was collected at five different constant CT speeds. The 2005 Shuttle-era CT rollout data had 27 acceleration response time histories from 9 triaxial accelerometers on the CT and the CT speed time history, which were recorded at five different CT speeds with durations ranging from 15 min and 20 min [8]. The 2005 Shuttle-Era CT transporting the MLP rollout data included the same data suite as the CT rollout data with an additional 36 acceleration response time histories from 12 triaxial accelerometers on the MLP, which were recorded at five different CT speeds with durations of around 10 minutes [8]. Previous analyses of these rollouts have been used to improve the accuracy of the CT and MLP FEM's [15, 16]. Spectral Density plots showed that these acceleration response time histories were dominated by the CT shoe and roller crossing harmonics. Direct application of OMA time-domain or frequency-domain techniques to these acceleration response time histories yielded no useful modal characteristics. Previous applications of OMA techniques to these rollout data sets were completed in August 2018 and discovered that a significant amount of harmonic reduction processing was needed to remove the CT harmonics before any attempt at using OMA techniques could be made.

ISVV_010 ROLLOUT DATA AND ENVIRONMENT

The ISVV-010 rollout instrumentation set consisted of 337 accelerometers on the ML, 40 accelerometers on the CT, 4 CT JEL pressures (one for each truck), CT Speed, and anemometer data collected at the top of the ML Tower (i.e., wind speed and direction, pressure, humidity, temperature, etc.). The modal pretest analysis for the ML modal test showed that these 377 accelerometers were sufficient to identify the target modes of the ML on CT test configuration based upon a cross-orthogonality criteria [9]. The ML modal test ML on CT test configuration had the CAA extended, while for the ISVV-010 rollout the CAA was retracted and rotated back to be alongside the ML Tower. Therefore the modes for these two configurations while having some similarities are different. The 337 ML acceleration channels were acquired with the SLS Mobile Data Acquisition System (MDAS) and the 45 CT channels were acquired with the CT Data Acquisition System (CTDAS). Both data acquisition systems operated at different sampling rates, but were Inter-Range Instrumentation Group timecode B (IRIGB) time synchronized. However, for still unknown reasons, the MDAS and CTDAS time histories were not fully time synchronize resulting in a significant amount of effort expended after the rollout to manually time synchronize them. The 337 ML accelerometers were comprised of both low noise low frequency (MDAS_Low) and high noise high frequency (MDAS_High) accelerometer types. The 40 CT accelerometers were a single type of accelerometer, but different from those on the ML. These ML and CT accelerometers, MDAS and CTDAS, were the same accelerometers used for the ML modal test that immediately preceded the ISVV-010 rollout. The ML on CT ISVV-010 rollout configuration was nearly identical to the ML on CT ML modal test configuration with the exception that the CAA was retracted and rotated back out of the way beside the ML Tower for the ISVV-010 rollout.

Figure 11 shows the test display model (TDM) with the locations and orientation of the ML and CT accelerometers. For this study, this TDM was also used to animate the OMA extracted test mode shapes. It has become increasingly popular to partially back expand test mode shapes to a larger set of grid points or even to back expand to the full FEM grid points. Caution should be applied when doing so because small errors in the test mode shapes, due to ambient noise, sensor noise, and nonlinearities in the test article, combined with differences between the FEM and the hardware will lead to back expanded mode shapes that erroneously indicate either deficiencies in the test instrumentation or FEM. If the animation of the test mode shapes back expanded so there are all three translational DOF at each instrument location is insufficient for the test engineer to visually interpret them, then it is recommended the instrumentation set be revised. For this study a Test Analysis Model (TAM) was not available so the OMA identified test mode shapes were not back expanded. Fortunately, the ML and CT accelerometer set had sufficient spatial resolution that it allowed the unexpanded OMA identified test mode shapes to adequately display the motion of the fundamental modes.

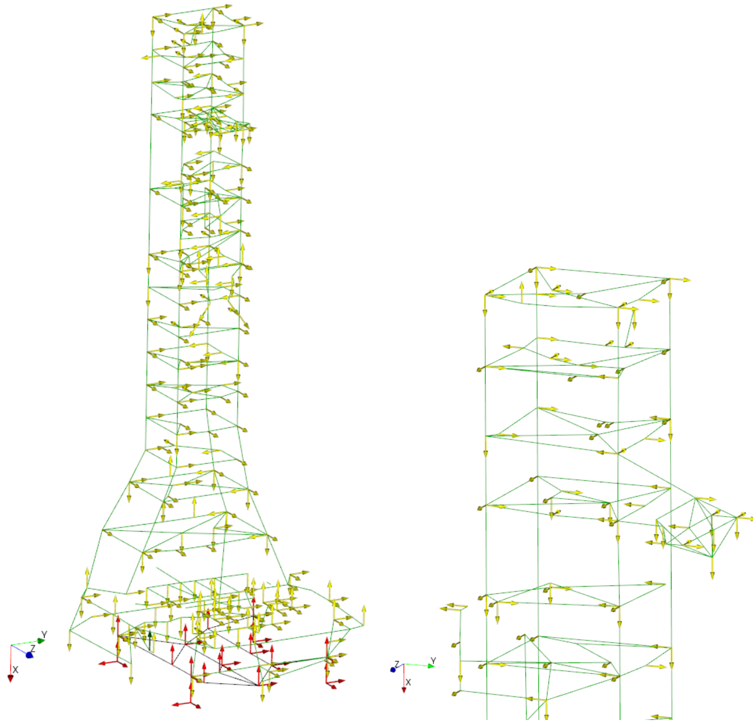

Figure 11. Test Display Model Showing Accelerometer Locations and Orientations on the ML and CT (left), and Close Up View of the Upper Portion of the ML Tower and Crew Access Arm (right).

It should be noted that the ML also has an independent dedicated set of permanently installed instrumentation that includes accelerometers and strain gages whose purpose is to measure responses during prelaunch and liftoff. This independent set of ML instrumentation was recorded on a separate independent data acquisition system during ISVV-010 rollout analysis. A separate modal pretest analysis was performed for the ISVV-010 using this independent set of instrumentation combined with the CT accelerometers [18]. Unfortunately, complete sets of this data were not available and their analysis will not be addressed in this paper.

The ISVV-010 rollout data consisted time histories collected over eight approximately one hour long non-overlapping time intervals, which contained the time histories of the ML and CT accelerometers, CT JEL pressures, and CT speed. Each of these data sets had the time histories time synchronized and down sampled to a common sampling frequency. These eight data sets spanned the entire rollout event from when the ML on CT started to first move inside the VAB until it reached Launch Pad 39B gate. The anemometer data, measured at the top of the ML Tower, was recorded on a separate data acquisition. Figure 12 shows the ISVV-010 rollout CT speed, ground wind speed, and ground wind direction, and the approximate breakdown of the eight rollout data sets. Figure 13 shows the same thing, but with the 10 second moving averaged ground wind speed and direction. Figure 14 shows a waterfall plot of the ground winds speed showing that wind gusts to be broadband and no significant tones present, which is consistent with ground winds turbulent gust models used in rollout, prelaunch, and liftoff analysis. The ground wind direction remained fairly constant during the rollout and there were significant periods where the ground winds were essentially still.

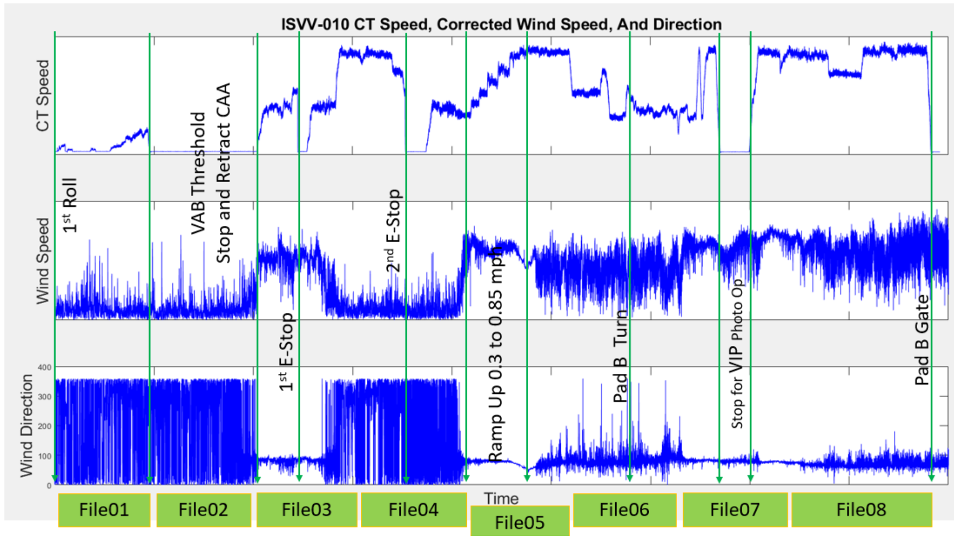

Figure 12. ISVV-010 Rollout Data: CT Speed (top), Ground Wind Speed (middle), Ground Wind Direction (bottom).

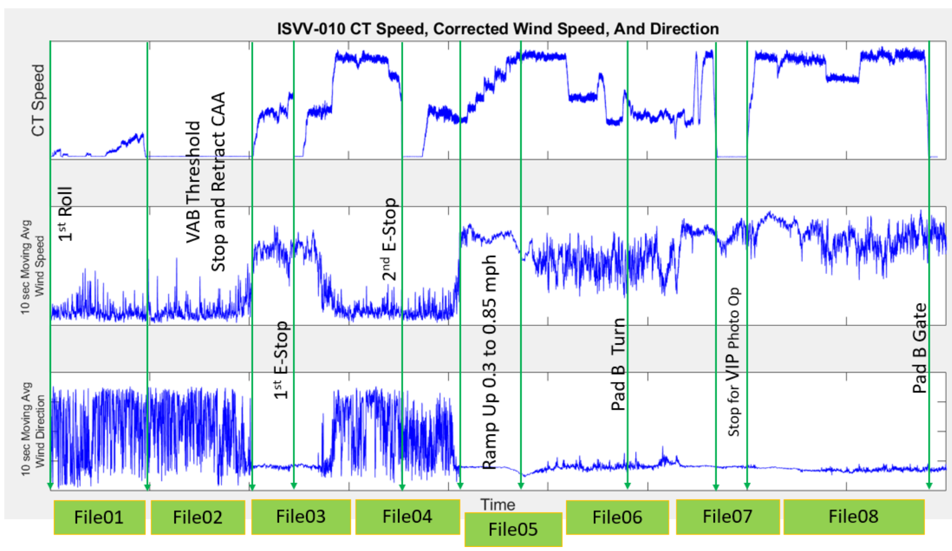

Figure 13. ISVV-010 Rollout Data: CT Speed (top), Average Ground Wind Speed (middle), Average Ground Wind Direction (bottom).

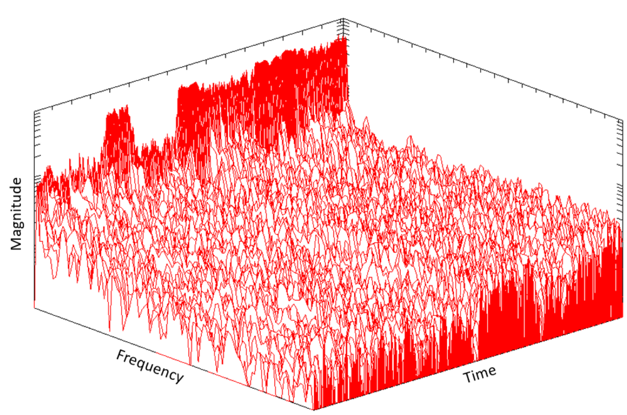

Figure 14. ISVV-010 Rollout Ground Wind Speed PSD Waterfall Plot.

ISVV-010 OMA Analysis Procedure

Time-domain and frequency-domain data quality checks were performed on the time synchronized acceleration time histories to identify potentially bad or questionable channels. Initial time-domain data quality checks included visual inspections of the time histories looking for data dropout, underflow (i.e., digitization error), overflow (i.e., clipping), asymmetries, excessive low frequency drifting, excessive transients, ringing, and other unexpected behaviors. Acceleration time histories that had overall amplitude levels that were out of family with what would be expectedly similar acceleration time histories potentially indicated scaling or noise issues. Scaling issues could be due to incorrect sensitivities entered into the data acquisition system channel table. Standard statistics (e.g., mean, max, min, standard deviation, kurtosis, and crest factor) were also computed and reviewed. Next frequency-domain data quality checks were performed using Power Spectral Densities (PSD's) (Auto Spectral Densities (ASD's)) computed on the acceleration time histories and again comparing PSD magnitudes of expectedly similar acceleration time histories was used to identify potentially bad or questionable channels. PSD's were also inspected to see if they possessed distinct resonance peaks at the expected ML on CT modal frequencies, CT harmonics, and 60 Hz harmonics due to electronic noise. These PSD's were also compared to the accelerometers manufacture's specified sensor noise PSD's to obtain a preliminary estimate of the Signal-to-Noise Ratio (SNR) on each channel. PSD waterfall plots were used in determining stationarity (i.e., time invariant behavior) and nonstationarity (e.g., transients, time dependent behavior, etc.) characteristics of each acceleration time history.

The time synchronized acceleration response time histories were then bandpass filtered and down sampled to a lower sampling frequency to prevent out-of-band high frequency content from obscuring what was going on in the frequency range of ML on CT fundamental modes. This also removed the very low frequency signal drift, which produced artificially high the amplitudes in the Spectral Densities leading to artificially high magnitudes at very low frequency in SVD of the SDM, which obscured the peaks of the lowest frequency ML on CT fundamental modes. This also reduced the computational burden on the OMA software. This bandpass filtering was accomplished using a digital 8^{th} order Butterworth band pass filter. To increase the steepness of the rollup and rolloff and to eliminate phase distortion, the time histories were passed forwards and backwards through this digital filter twice. The validity of this bandpass filter was verified by comparing PSD's computed on the bandpass filtered acceleration time histories to those of the unfiltered acceleration time histories, such as that shown in Figure 15. Figure 16 show the bandpass filtered acceleration time histories for a triaxial group of accelerometers at the top of the ML Tower. The bandpass filtering produced transients at the beginning and ending of the bandpass filtered acceleration time histories due to the transient behavior (i.e., impulse response characteristics) of the band pass filter. Figure 17 compares an unfiltered and bandpass filtered acceleration time histories displaying this transient behavior at the start of it. When choosing a filter, the analyst should not only take into account its frequency characteristics (i.e., ripple in the pass band, rolloff and rollup slope, phase distortion, etc.), but should also consider its time-domain characteristics (i.e., impulse and step response, length of filter, etc.). In this case, with a digital filter, by running time histories forwards and backwards through the filter eliminates phase distortion, but comes at the cost of accentuating the filter transients at the beginning and ending of the time histories. If transients cannot be tolerated, butterflying techniques can be used on the time histories prior to filtering, which will eliminate transients at the beginning and ending of the bandpass filtered time histories. For this study, the transients had an insignificant duration with respect to the total duration, so that excluding them did not impact the OMA analysis.

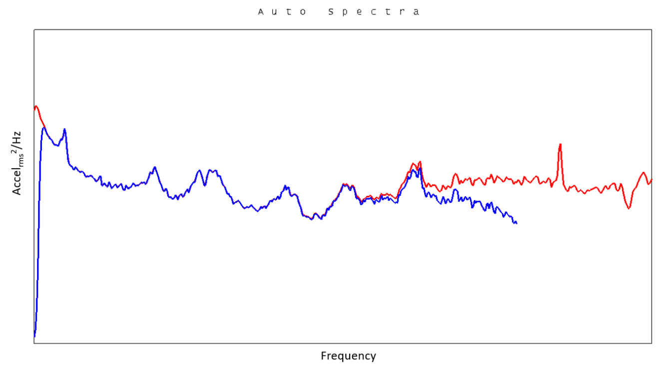

Figure 15. PSD Comparison: Unfiltered (red), Bandpass Filtered (blue).

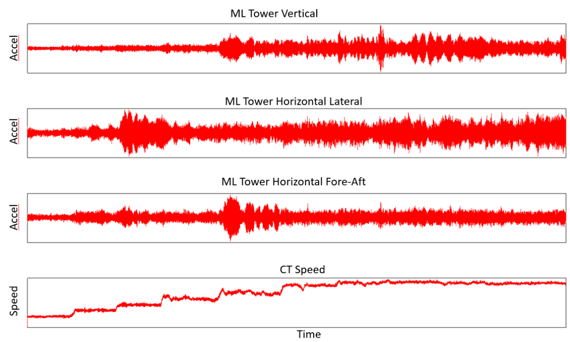

Figure 16. Top of ML Tower Bandpass Filtered Acceleration Time Histories.

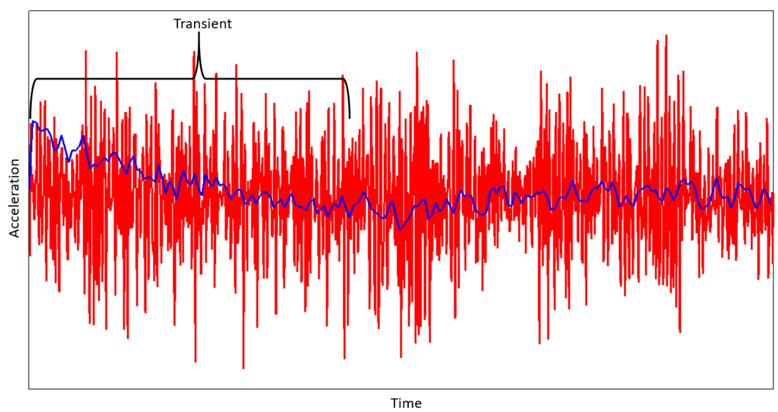

Figure 17. Acceleration Time Histories: Unfiltered (red) and Bandpass Filtered Displaying Initial Transient (blue).

Time-domain data quality checks were then performed on these bandpass filtered time histories. The time-domain checks included those performed on the original unfiltered time histories, but also identified portions of the time histories that had transients produced by the bandpass filtering, which were excluded from OMA analysis. Large unexplained spurious excursions in the acceleration response time histories were observed in the data. Some appeared to be due to intermittent connection issues (i.e., sharp step followed by monotonic exponential decay), while others appeared to be true impulses generated by something or someone impacting the structure. These excursions were removed by zeroing out their amplitude as shown in Figure 18.

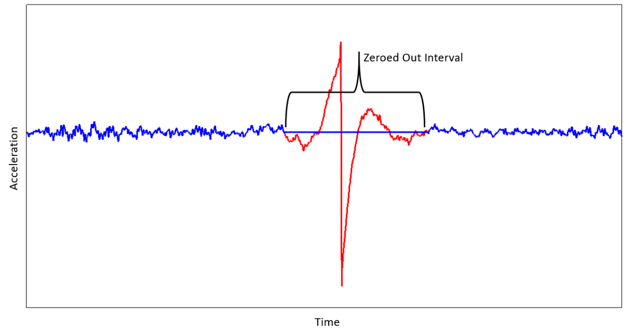

Figure 18. Removing Large Unexplained Spurious Excursions: Original Time History with Excursion (red) and Modified Time History with the Excursion Zeroed Out (blue).

Next frequency-domain data quality checks were performed using PSD's computed on the bandpass filtered acceleration time histories, excluding the transients produced by the bandpass filter, similar to those performed on the unfiltered time histories. PSD's computed on the File05 MDAS low frequency low noise, MDAS high frequency high noise, and CTDAS accelerometer time histories showed their amplitudes were well above the manufacturer's maximum sensor noise floor over the frequency range of interest. This verified that the MDAS and CTDAS accelerometer channels had an adequate SNR for this data set where the CT was moving. Therefore all of the MDAS and CTDAS accelerometers, excluding a few identified potentially bad channels, were included when OMA techniques were applied to the six time intervals analyzed that had the CT moving. However, when the CT was stopped, while all of MDAS low frequency low noise and most of the CTDAS accelerometers still possessed an adequate SNR, many of the MDAS high frequency high noise accelerometers did not. Therefore the MDAS high frequency high noise accelerometers were not included when OMA techniques were applied to the two time intervals analyzed that had the CT stopped.

Projection Channels are used to reduce the size of the SDM and minimize the computational burden in computing the SVD of the SDM and in implementing the OMA time-domain identification techniques. Instead of the SDM being a matrix with the number of rows and columns being equal to the total number of data channels, the SDM is formed having its number of rows equal to the number of Projection Channels and columns equal to the total number of data channels. Projection Channels are data channels that contain "unique" information with respect to all data channels and typically are relatively small in size even for data sets having a large number of data channels.

Several different sets of Projection Channels were studied using the File05 data set in order to determine the optimal set. First the OMA software was allowed to automatically select the Projection Channels, which produced three channels: 3200659X+ (top of the ML Tower, Level 345, vertical direction), 3200100Y+ (ML Tower Level 260, horizontal lateral), and 341009Y+ (CAA inboard end, horizontal lateral). This resulted in no harmonics being detected and produced an SVD of the SDM with well-shaped peaks. However, the SVD peak for the ML Tower 1st lateral bending Z-Axis (fore-aft) mode, which was the lowest frequency mode, was not as well defined as the second SDV peak for the ML Tower 1st lateral bending Y-Axis (lateral) mode.

Next 20 Projection Channels were manually selected to try and improve the SVD peak for the ML Tower 1st lateral bending Z-Axis (fore-aft) and to hopefully get better participation of the ML Deck and CT motion. These 20 Projection Channels included a triaxial group of accelerometers at the top of the ML Tower, Level 345, one biaxial group of accelerometers and one uniaxial accelerometer on the CAA, two triaxial groups and one biaxial group of accelerometers on the CT, and six uniaxial accelerometers on the ML Deck with three in the vertical (i.e., X-Axis), one in the lateral (i.e., Y-Axis), and two in the fore-aft (i.e., Z-Axis) directions. However, this resulted in a significantly degraded SVD that did not have well defined SVD peaks (i.e., very choppy or noisy appearance) that the SVD with the automatically selected 3 Projection Channels. In addition a large number of CT harmonics were detected.

Next 5 Projection Channels were manually selected, which did not include any accelerometers on the CT to hopefully minimize the effect of the CT shoe and roller crossing harmonics. These 5 Projection Channels had a triaxial group of accelerometers at the top of the ML Tower, Level 345, 3200659X+, Y+, Z+, one uniaxial accelerometer on the CAA 3410009Y+ (lateral), and one uniaxial accelerometer on the ML Deck 3002531X- (vertical). While no harmonics were automatically detected, the SVD was still significantly noisier than the SVD of the automatically selected 3 Projection Channels. The PSD's of these Projection Channels showed that the uniaxial accelerometer 3002531X- on the ML Deck did not have any resonance peaks that were not already present in the four other Projection Channels and had no resonance peaks above 3 Hz. Therefore the uniaxial accelerometer 3002531X- on the ML Deck not only did not provide any unique information beyond the four other Projection Channels, but was also introducing numerical noise to the process and therefore was a poor choice for a Projection Channel.

Based upon the above findings, four Projection Channels were selected for this study, which included the three automatically selected Projection Channels supplemented with one uniaxial accelerometer at the top of the ML Tower, Level 345, 3200569Z+ (fore-aft), which along with 3200569X+ (fore-aft) placed a biaxial group at the top of the ML Tower. This resulted in an SVD that had peaks that were slightly noisier than the peaks of the SVD for the three automatically selected Projection Channels, but had a much stronger SVD peak corresponding the ML Tower 1st lateral bending Z-Axis (fore-aft) mode. Figure 19 shows the physical layout and orientation of these four Projection Channels. This study showed that the appropriate selection of the Projection Channels plays a critical role in successfully applying OMA techniques, especially when dealing with a very large channel count.

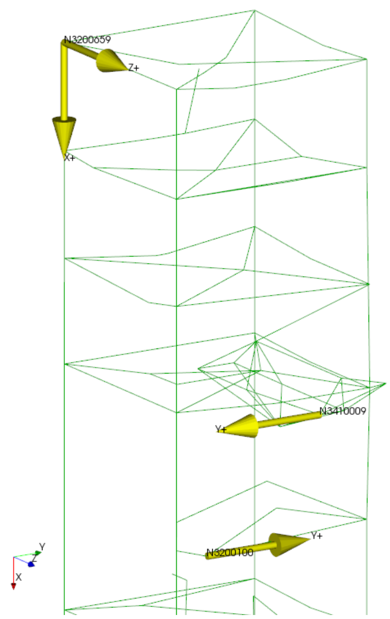

Figure 19. Physical Layout and Orientation of the Selected Four Projection Channels.

Unexpectedly it was discovered that applying OMA time-domain and frequency domain techniques to time intervals where the CT speed was constantly varying, but not varying too drastically (e.g., during an Emergency Stop (E-Stop)), mitigated the detrimental effects of the CT shoe and roller crossing harmonics, and eliminated the need for performing harmonic reduction on the bandpass filtered time histories. OMA time-domain and frequency domain techniques were successfully used to identify modes from a total of six time intervals when the CT was moving with its speed constantly varying. These analyzed time intervals excluded time intervals were large transient events were taking place (i.e., during an E-Stop). These time intervals had durations ranging from 21 minutes to 70 minutes. OMA techniques were able to identify the highest number of modes from the File05 data set, which had a "stair step" pattern CT speed profile and the greatest overall variation in the CT speed while the CT was moving. Figure 20 shows the File05 CT speed profile.

Figure 20. File 05 CT Speed Profile.

Initially the order of application of the OMA mode identification techniques was to first use the frequency-domain techniques (Frequency Domain Decomposition (FDD), Enhance Frequency Domain Decomposition (EFDD), Curve-fit Frequency Domain Decomposition (CFDD) followed by the time-domain techniques (Stochastic Subspace Identification with Unweighted Principal Component (SSI-UPC) and/or SSI Extended Unweighted Principal Component (SSI-UPCX)). The pitfall with this approach was that there were a large number of SVD peaks that looked like they could correspond to ML on CT fundamental modes. It was very tempting to pick most of the SVD peaks, which ended up generating a very large set of pole estimates, which unfortunately did not correspond to actual modes and slowed down the mode identification process.

Instead the order of application of the OMA mode identification techniques that was used for the majority of the analysis started with the time-domain SSI-UPCX technique, which was followed with CFDD technique to verify the SSI-UPCX identified modes. Then the CFDD technique was judiciously used to identifying additional modes corresponding to dominant SVD peaks, which had positive modal damping that the SSI-UPCX technique had missed for whatever reason. Next the EFDD technique was used to verify the SSI-UPCX and CFDD identified modes and then identifying additional modes corresponding to dominant SVD peaks, which had positive modal damping that the SSI-UPCX and CFDD techniques had missed for whatever reason. Finally the FDD technique was used to verify the SSI-UPCX, CFDD, and EFDD identified modes and adding just a few pole estimates for dominant SVD peaks not already captured that were believed to be due to harmonics. This resulted in a significantly smaller and higher quality set of candidate modes and dominant harmonics. The SSI-UPCX parameters were varied in an attempt to and get “stable” pole estimates corresponding to some of the initially missed SVD peaks. While this could be done to get a larger candidate mode set, these additional modes always ended having unrealistic modal damping, overly complex mode shapes, and poor quality mode shapes, and therefore did not produce useful results.

Figure 21 shows the SSI-UPCX stabilization diagram computed on the File05 bandpass filtered acceleration response time histories, which has a well-developed racetrack pattern of the pole estimates corresponding to most of the dominant SVD peaks. Figure 22 shows the high quality CFDD fits of the first two SVD peaks. Figure 23 shows the high quality EFDD fit of the second SVD peak.

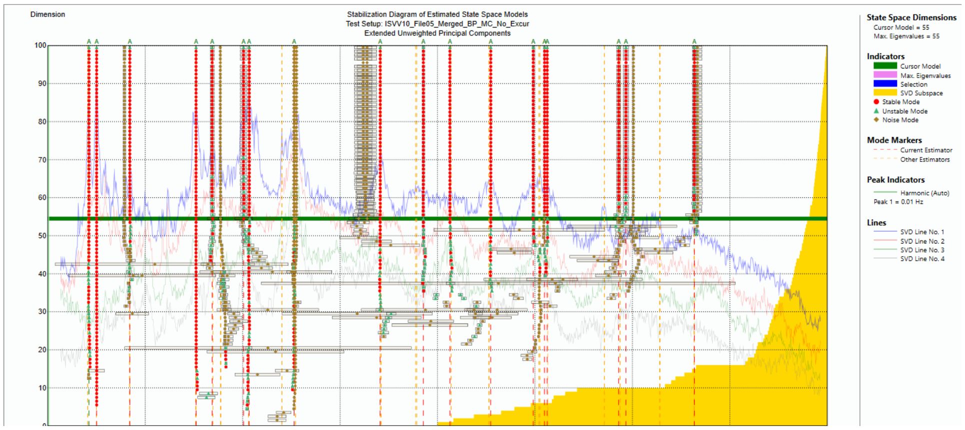

Figure 21. File05 SSI-UPCX Stability Diagram.

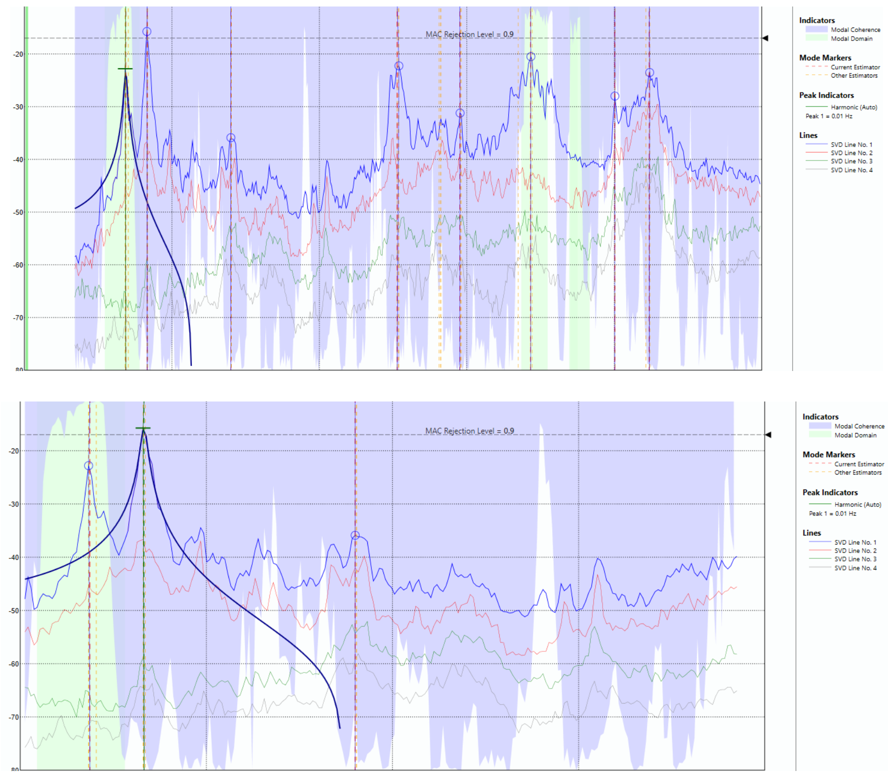

Figure 22. File05 SVD CFDD Fits: First SVD Peak (top) And Second SVD Peak (bottom).

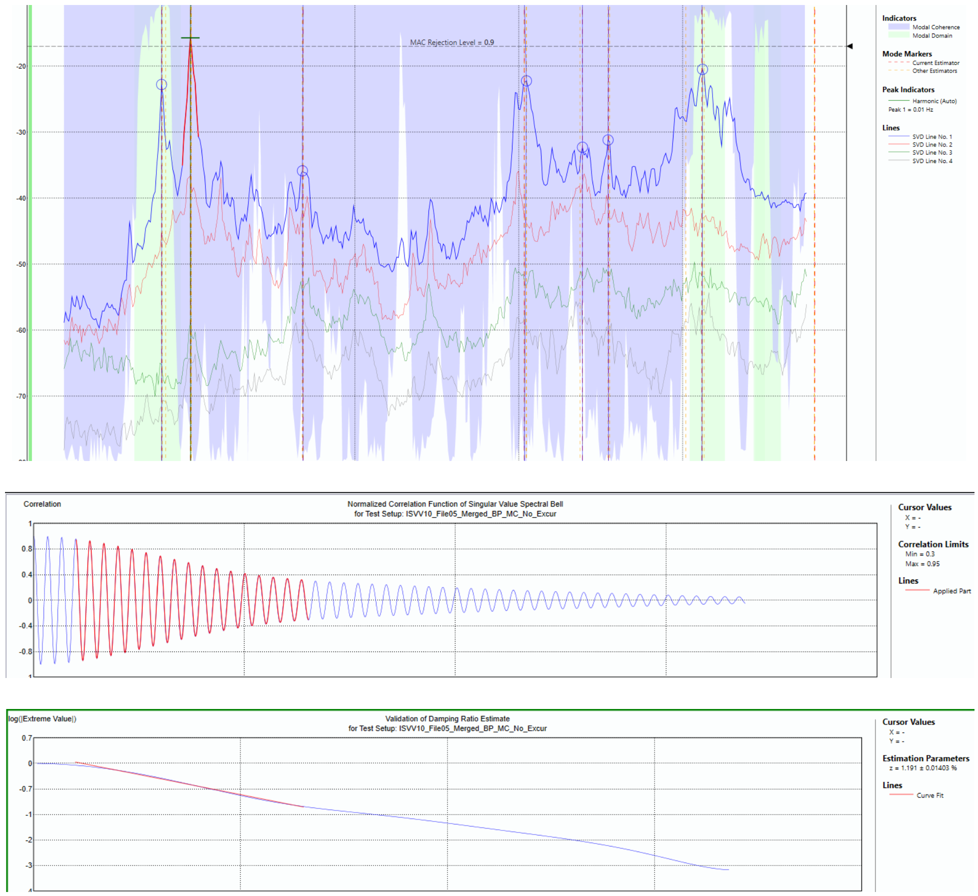

Figure 23. File05 SVD of SDM: EFDD Fits Of Second SVD Peak.

For each test run, the modes identified by each OMA technique had their mode shapes compared using a cross Modal Assurance Criteria (XMAC). This was necessitated due to not having a Test Analysis Model (TAM) mass matrix available for being able to compute cross orthogonalities (XORTHO). Mode shapes were considered very well matched for XMAC values greater than or equal to 0.9 and well matched for the XMAC values greater than or equal to 0.87 and less than 0.9. The NASA-STD-5002 criteria for mode shapes being well matched is their XORTHO value being greater than 0.9 [19], which corresponds to an XMAC value of 0.81. Note that an XMAC value of 0.87 corresponds to a XORTHO value of 0.93. The more conservative XMAC criteria of being greater than or equal to 0.87 was chosen to hopefully avoid including undetected harmonics in the final mode sets. From these XMAC comparisons, a table of preliminary final mode set from each time interval analyzed was constructed with the candidate modes with confidence in the modes a function of the number of techniques that identified them. Figure 24 shows the first 15 modes of the File05 preliminary mode set.

(green)	= High confidence in this modes actually existing (i.e. identified by all methods).
(blue)	= Medium confidence in this modes actually existing (i.e. identified by all frequency domain techniques or SSI-UPCX and two other frequency domain techniques).
(yellow)	= Low confidence in this mode actually existing (i.e. only identified by two methods).
(pink)	= Very low confidence in this mode actually existing (i.e. only identified by one method).

Number of high confidence modes =	6
Number of medium confidence modes =	10
Number of low confidence modes =	2
Number of very low confidence modes =	12
Total number of modes =	30

Preliminary Final Mode Set																
					CFDD			EFDD				FDD				
Mode #	Method	Freq	Damp	Mode Shape Description	Freq	Damping	SSI/CFDD XMAC	Freq	Damping	SSI/EFDD XMAC	CFDD/EFDD XMAC	Freq	SSI/FDD XMAC	CFDD/FDD XMAC	EFDD/FDD XMAC
1	SSI-UPCX	1.00	1.00	ML Tower 1st Lateral Bending Z-Axis, CAA Translation Z-Axis In-Phase.	0.975	0.35	1.00	0.97	0.18	1.00	1.00	0.97	0.99	1.00	1.00
2	SSI-UPCX	1.19	0.14	ML Tower 1st Lateral Bending Y-Axis,.	1.182	0.22	1.00	1.18	0.26	1.00	1.00	1.18	1.00	1.00	1.00
3	CFDD	1.99	0.11	ML Tower 1st Lateral Bending Z-Axis, ML Deck Translation Z-Axis.	NA	NA	NA	1.99	0.18	NA	1.00	1.99	NA	0.98	0.98
4	SSI-UPCX	1.99	1.27	ML Tower 1st Lateral Bending Z-Axis, ML Deck Translation Z-Axis.	NF	NA	NA	NF	NA	NA	NA	NF	NA	NA	NA
5	SSI-UPCX	3.60	0.15	ML Tower 1st Torsion, CSITU & CSFSU Translation Y-Axis Out-of-Phase With Tower Torsion.	3.589	0.15	0.99	1.517	0.27	0.99	1.00	1.523	1.00	0.98	0.98
6	SSI-UPCX	3.99	1.60	ML Tower 2nd Lateral Bending Z-Axis, ML Deck And CT Translation Z-Axis And Rotation About Y-Axis, VSS Translation, CSITU Y-Axis Translation.	NF	NA	NA	NF	NA	NA	NA	NF	NA	NA	NA
7	EFDD	4.01	0.05	ML Tower 2nd Lateral Bending Z-Axis, ML Deck And CT Translation Z-Axis And Rotation About Y-Axis, VSS Translation, CSITU Y-Axis Translation.	NA	NA	NA	NA	NA	NA	NA	NF	NA	NA	NA
8	CFDD	4.19	0.03	ML Tower 2nd Lateral Bending Z-Axis And 1st Torsion, ML Deck And CT Translation Z-Axis And Rotation Y-Axis, ML Deck Rotation About X-Axis.	NA	NA	NA	4.20	0.05	NA	1.00	4.20	NA	0.98	0.98
9	SSI-UPCX	4.75	1.12	ML Tower 2nd Lateral Bending Y & Z-Axis, ML Tower 1st Torsion, ML Deck & CT Rotation About Y-Axis, VSS Translation.	NF	NA	NA	NF	NA	NA	NA	NF	NA	NA	NA
10	SSI-UPCX	4.89	0.27	ML Tower 2nd Lateral Bending Z-Axis.	4.873	0.19	0.99	4.87	0.39	0.99	1.00	4.88	0.99	0.99	0.99
11	CFDD	5.68	0.02	ML Tower Translation X-Axis (i.e. Vertical Motion), ML Deck & CT Rotation About Y-Axis, VSS Translation X-Axis (i.e. Vertical Motion) Of Both Ends In-Phase With ML Tower Bending.	NA	NA	NA	5.68	0.184	NA	1.00	5.68	NA	0.99	0.99
12	SSI-UPCX	5.98	0.32	ML Tower Translation X-Axis (i.e. Vertical Motion), ML Tower 3rd Lateral Bending Y & Z-Axis, ML Deck & CT Rotation About Y-Axis, CAA & Umbillicals.	NF	NA	NA	NF	NA	NA	NA	NF	NA	NA	NA
13	CFDD	6.01	0.01	ML Tower Translation X-Axis (i.e. Vertical Motion), ML Tower 2nd Lateral Bending Y & Z-Axis, ML Deck & CT Rotation About Y-Axis, CAA & Umbillicals.	NA	NA	NA	6.02	0.156	NA	1.00	6.02	NA	0.98	0.98
14	SSI-UPCX	8.07	0.25	CAA Translation Y-Axis.	8.074	0.12	0.93	8.07	0.20	0.93	1.00	8.10	0.95	0.96	0.96
15	SSI-UPCX	9.12	1.20	ML Tower 3rd Lateral Bending Z-Axis, ICPSU & CSFSU Translation Z-Axis Out-of-Phase With ML Tower.	8.954	0.22	0.90	8.96	0.39	0.90	1.00	8.93	0.91	0.99	0.99

Figure 24. File05 Preliminary Final Mode Set (Modes 1 – 15 only) (normalized to lowest frequency mode).

The preliminary final mode sets for when the CT was moving then had their mode shapes compared again using a XMAC criteria to obtain the final set of modes. This was done believing that modes identified from different test runs, which had different CT speeds, which matched further helped to avoid selecting modes that were actually due to a harmonic. However, unexpectedly it was found the modes identified from File04 from 10 seconds to 1710 seconds had very poor agreement with the modes extracted from the five other time intervals based upon XMAC values. Figure 25 shows the CT speed profiles for all six time intervals analyzed when the CT was moving. The File04, from 10 seconds to 1710 seconds, CT Speed profile was in family with the CT speed profiles of the five other time intervals. However, for File04 from 10 seconds to 1710 seconds, the ground winds were minimal, while there were significantly stronger ground winds during the other time intervals. Furthermore, excluding test DOF on the umbilicals, VSS, and the CAA, significantly improved the XMAC between the File04 modes and those of the five other time intervals the CT was moving. This indicated the relative motion of the CAA, umbilicals, and VSS was the differentiating factor in these mode shapes. This indicates the ML on CT modes, when the CT was moving, were dependent upon the ground winds speed. Moreover, this indicates the major contributors to this nonlinear response were the CAA, umbilicals, and VSS.

The final mode set for when the CT was moving did not include the File04 from 10 seconds to 1710 seconds preliminary final modes, but was drawn from the five other time intervals analyzed when the CT was moving. The final modal frequencies and modal damping values taken from the average values and the mode shapes were taken from the Fil05 preliminary final modes since all five preliminary final modes had extremely high XMAC values. Figure 26 and Figure 27 shows the preliminary final modes that made up the CT moving final mode set of 15 modes and 2 harmonics, which have frequencies identified as harmonics when the CT was stopped and have extremely low modal damping values.

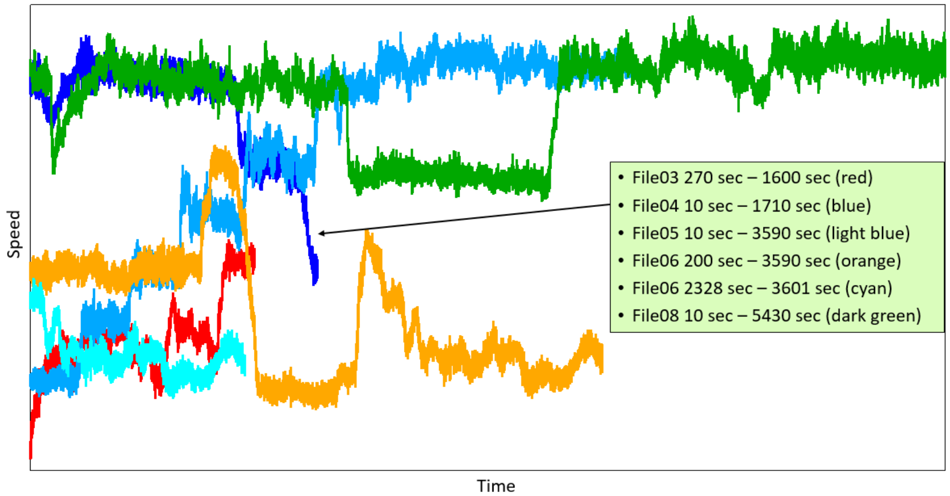

Figure 25. CT Speed Profiles for the Six Time Intervals Analyzed with CT Moving.

Mode Shape Description	File05_10_3590_04		File03_270_1600				File06_200_3590 (6a)				File06_2328_3601 (6b)				File08_10_5430				Final									
	Freq	Damp	Freq	Damp	XMAC	Freq Diff (%)	Freq	Damp	XMAC	Freq Diff (%)	Freq	Damp	XMAC	Freq Diff (%)	Freq	Damp	XMAC	Freq Diff (%)	Avg Freq	Min Freq	Min Freq (%)	Max Freq	Max Freq (%)	Avg Damp	Min Damp	Min Damp (%)	Max Damp	Max Damp (%)
ML Tower 1st Lateral Bending Z-Axis, CAA Translation Z-Axis In-Phase, ICPSU & CSFSU Translation Z-Axis Out-of-Phase, ML Deck Motion.	1.00	1.0	0.98	0.6	99	-2.2	1.02	0.7	100	1.8	0.98	0.3	100	-1.9	1.07	2.0	99	7.5	**1.01**	0.98	-3.3	1.07	6.4	**0.9**	0.3	-64	2.0	113
ML Tower 1st Lateral Bending Y-Axis, ICPSU and CSFSU Translation Z-AxisOut-of-Phase, ML Deck Motion.	1.19	0.1	1.18	0.1	100	-0.2	1.19	0.1	100	-0.1	1.16	0.4	99	-1.8	1.19	0.1	100	0.0	**1.18**	1.16	-1.4	1.19	0.5	**0.2**	0.1	-60	0.4	126
ML Tower 1st Torsion, CSITU & CSFSU Translation Y-Axis Out-of-Phase With Tower Torsion.	3.60	0.2	3.60	0.1	99	0.0	3.59	0.1	98	-0.4	3.62	0.3	99	0.6	3.63	0.3	98	0.7	**3.61**	3.59	-0.6	3.63	0.5	**0.2**	0.1	-66	0.3	73
ML Tower 2nd Lateral Bending Z-Axis, VSS Motion, ICPSU & CSFSU Translation Z-Axis Out-of-Phase, CSITU Translation Y-Axis, ML Deck & CT Translation Z-Axis.	4.89	0.3	4.86	0.8	95	-0.6	4.83	0.3	98	-1.3	4.86	1.0	92	-0.6	4.75	0.6	97	-2.8	**4.84**	4.75	-1.8	4.89	1.1	**0.6**	0.3	-55	1.0	65
ML Tower 2nd Lateral Bending Y-Axis, Translation X-Axis, ML Deck And CT Rotation About X-Axis, ML Deck Bending.	6.01	0.0					6.51	0.0	90	7.6					6.11	0.1	89.5	1.7	**6.21**	6.01	-3.2	6.51	4.8	**0.1**	0.0	-76	0.1	150
CAA Translation Y-Axis.	8.07	0.2					8.17	0.4	98	1.2	8.17	0.3	98	1.2	8.02	0.3	100	-0.6	**8.09**	8.02	-0.8	8.17	1.0	**0.3**	0.2	-21	0.4	18
ML Tower 3rd Lateral Bending Z-Axis, ICPSU & CSFSU Translation Z-Axis Out-of-Phase With ML Tower.	9.12	1.2	9.07	0.5	97	-0.5	9.12	0.5	98	0.0					9.16	1.4	99	0.5	**9.13**	9.07	-0.7	9.16	0.3	**1.0**	0.5	-56	1.4	32
ML Tower 3rd Lateral Bending Y-Axis, CAA Rotation About Z-Axis Out-of-Phase, VSS Motion, ML Deck & CT Translation Y-Axis.	9.77	0.5					9.88	0.9	92	1.2	9.76	1.0	94	-0.1	9.70	0.0	99	-0.7	**9.78**	9.70	-0.8	9.88	1.1	**0.6**	0.0	-99	1.0	64
ML Tower 3rd Lateral Bending Z-Axis, CAA Translation X-Axis, ICPSU & CSFSU Translation Z-Axis Out-of-Phase With ML Tower, VSS Motion, ML Deck & CT Translation Z-Axis and Bending.	9.79	0.0													9.94	0.0	98	1.5	**9.87**	9.79	-0.8	9.94	0.8	**0.0**	0.0	-32	0.0	32
ML Tower 2nd Torsion, CAA Translation X-Axis, ML Deck & CT Rotation About X-Axis and Bending.	10.71	0.1													10.72	0.1	96	0.1	**10.72**	10.71	0.0	10.72	0.0	**0.1**	0.1	-1	0.1	1
ML Tower 2nd Torsion, CSITU Translation Y-Axis In-Phase, ML Deck & CT Rotation About X-Axis and Bending.	10.75	0.3					10.75	0.2	96	0.0	10.85	0.4	89	0.9	10.73	0.5	100	-0.2	**10.77**	10.73	-0.4	10.85	0.7	**0.3**	0.2	-38	0.5	31
CAA Translation X-Axis, CT Bounce Mode Out-of-Phase.	11.79	0.4					11.94	0.4	95	1.2	12.12	0.3	93	2.8	11.76	0.4	99	-0.3	**11.90**	11.76	-1.2	12.12	1.8	**0.4**	0.3	-16	0.4	15

= High confidence in this modes actually existing (i.e. identified by all methods).
= Medium confidence in this modes actually existing (i.e. identified by all frequency domain techniques or SSI-UPCX and two other frequency domain techniques).
= Low confidence in this mode actually existing (i.e. only identified by two methods).
= Very low confidence in this mode actually existing (i.e. only identified by one method).

Figure 26. CT Moving Final Mode Set, Modes 1 - 12 (normalized to lowest frequency File05 mode).

Mode Shape Description	File05_10_3590_04		File03_270_1600				File06_200_3590 (6a)				File06_2328_3601 (6b)				File08_10_5430				Final										
	Freq	Damp	Freq	Damp	XMAC	Freq Diff (%)	Freq	Damp	XMAC	Freq Diff (%)	Freq	Damp	XMAC	Freq Diff (%)	Freq	Damp	XMAC	Freq Diff (%)	Avg Freq	Min Freq	Min Freq (%)	Max Freq	Max Freq (%)	Avg Damp	Min Damp	Min Damp (%)	Max Damp	Max Damp (%)	
CAA And CSFSU Translation X-Axis In-Phase, ML Deck Translation X-Axis In-Phase, CT Motion.	13.51	0.0													13.46	0.0	93	-0.4	**13.48**	13.46	-0.2	13.51	0.2	**0.0**	0.0	-48	0.0	48	**Harmonic?**
ML Tower X-Axis 2nd Longitudinal Mode (i.e. Top & Bottom ML Tower X-Axis Translation Out-of-Phase), CAA Translation X-Axis, CSFSU & ICPSU, ML Deck Motion, Dominant CT Z-Axis 1st Bending Out-of-Phase With Deck Motion.	14.04	0.8													13.64	0.7	92	-2.8	**13.84**	13.64	-1.4	14.04	1.4	**0.8**	0.7	-4	0.8	4	
CAA Translation X-Axis (i.e. Vertical Motion), ICPSU Translation Z-Axis, ML Tower 3rd Torsion, ML Tower Chair Rotation About the Z-Axis, CT Rotation About Y-Axis.	14.86	0.0					14.82	0.1	96	-0.3					14.84	0.0	93	-0.1	**14.84**	14.82	-0.1	14.86	0.1	**0.0**	0.0	-52	0.1	32	**Harmonic?**
CAA Translation X-Axis (i.e. Vertical Motion), ICPSU Translation Z-Axis, ML Tower 3rd Torsion, ML Tower Chair Rotation About the Z-Axis, CT Rotation About Y-Axis, CT Trucks Translation Z-Axis (Corners A&D Out-of-Phase With Corners B&C).	15.70	0.1					15.57	0.0	92	-0.8					15.64	0.1	98	-0.4	**15.64**	15.57	-0.4	15.70	0.4	**0.1**	0.0	-26	0.1	14	
CAA Translation X-Axis (i.e. Vertical Motion), ICPSU Translation Z-Axis, ML Tower 3rd Torsion, ML Tower Chair Rotation About the Z-Axis, CT Rotation About Y-Axis, CT Trucks Translation Z-Axis (Corners A&D Out-of-Phase With Corners B&C).	15.70	0.6													15.67	0.7	91	-0.2	**15.69**	15.67	-0.1	15.70	0.1	**0.6**	0.6	-8	0.7	8	

= High confidence in this modes actually existing (i.e. identified by all methods).
= Medium confidence in this modes actually existing (i.e. identified by all frequency domain techniques or SSI-UPCX and two other frequency domain techniques).
= Low confidence in this mode actually existing (i.e. only identified by two methods).
= Very low confidence in this mode actually existing (i.e. only identified by one method).

Figure 27. CT Moving Final Mode Set, Modes 13 – 15 and Two Harmonics (normalized to lowest frequency File05 mode).

Figure 28 shows the MAC of the CT moving final mode set. This shows good separation of modes at low frequency with gradually increasing coupling (i.e., higher off-diagonal values) with increasing frequency, which was expected due to the umbilicals in-phase and out-of-phase motion causing closely spaced modes. This poorer separation of the higher frequency modes was not unexpected because the layout and orientation of the MDAS and CTDAS accelerometers was selected based upon an ORTHO criteria. When a TAM becomes available, an ORTHO of the CT moving final mode set should be computed to verify separation of these modes.

			1	2	3	4	5	6	7	8	9	10	11	12	13	14	15	16	17
			1.00	1.16	3.53	4.74	6.12	7.95	8.98	9.60	9.70	10.53	10.58	11.70	13.26	13.60	14.58	15.37	15.42
100	1	1.00	100	8															
95	2	1.16	8	100															
90	3	3.53			100			7				7	5						
85	4	4.74				100	14		5										
80	5	6.12				14	100				8								
75	6	7.95			7			100											
70	7	8.98				5			100		76	5							
65	8	9.60								100									
60	9	9.70					8		76		100	22	17			6	8		
55	10	10.53			7				5		22	100	92		5				
50	11	10.58			5						17	92	100	5	8				
45	12	11.70											5	100	28	15	5		
40	13	13.26										5	8	28	100	22	29		13
35	14	13.60									6			15	22	100	26	5	14
30	15	14.58									8			5	29	26	100	24	50
25	16	15.37														5	24	100	71
20	17	15.42													13	14	50	71	100

Figure 28. MAC CT Moving Final Mode Set (modal frequencies normalized to 1st mode).

OMA techniques were also successfully used to identify modes when the CT was stopped, which did not possess the CT shoe and roller crossing harmonics. However, it should still be noted the JEL control system was still active and the diesel engines, generators, pumps, and other machinery were still in operating. Since the MDAS high frequency high noise accelerometers showed poor SNR, they were not included in this analysis. Two time intervals when the CT was stopped were analyzed, one after the 2nd E-Stop and during the very important person photography opportunity (VIP Photo Op), with both having a duration of eight minutes. While CT was stopped for more the twelve minutes both times, due to transients and ring down from the E-Stops present in the ML acceleration time histories and other things, only 8 minutes were considered to be sufficiently "stationary" and therefore selected for analysis. Figure 29 shows the preliminary final modes that made up the CT stopped final mode set that includes 6 modes and two harmonics.

	File04_1866_2348 (4b)		File07_2156_2624				Final										
Mode Shape Description	**Freq**	**Damp**	**Freq**	**Damp**	**XMAC**	**Freq Diff (%)**	**Avg Freq**	**Min Freq**	**Min Freq (%)**	**Max Freq**	**Max Freq (%)**	**Avg Damp**	**Min Damp**	**Min Damp (%)**	**Max Damp**	**Max Damp (%)**	
ML Tower 1st Lateral Bending Z-Axis, CAA Translation Z-Axis In-Phase, ICPSU & CSFSU Z-Axis Translation Out-of-Phase, VSS Motion, ML Deck Motion.	1.00	1.0	0.98	2.0	95	-1.7	**0.99**	0.98	-0.9	1.00	0.9	**1.5**	1.0	-33	2.0	33	
ML Tower 1st Lateral Bending Y-Axis, ICPSU & CSFSU & CSITU Translation Y-Axis Out-of-Phase, VSS Motion, ML Deck Motion.	1.18	0.0	1.20	1.9	99	1.8	**1.19**	1.18	-0.9	1.20	0.9	**1.0**	0.0	-96	1.9	96	
ML Tower 1st Torsion, ICPSU & CSITU & CSFSU Translation Y-Axis Out-of-Phase With Tower Torsion, ML Deck Rotation About	3.48	0.1	3.48	0.1	100	0.1	**3.48**	3.48	0.0	3.48	0.0	**0.1**	0.1	-5	0.1	5	
ML Tower 2nd Lateral Bending Z-Axis, CSFCU Translation Z-Axis Out-of-Phase, VSS Motion, ML Deck Motion, CT 1st Bending Z-Axis.	4.46	0.8	4.45	1.7	91	-0.4	**4.45**	4.45	-0.2	4.46	0.2	**1.2**	0.8	-36	1.7	36	
ML Tower 2nd Lateral Bending Y & Z-Axis, ML Tower Translation X-Axis, ICPSU & CSFSU & VSS Motion, ML Deck Motion, CT Rotation About Y-Axis.	6.83	0.5	6.87	1.8	99	0.6	**6.85**	6.83	-0.3	6.87	0.3	**1.1**	0.5	-55	1.8	55	
CAA Translation Y-Axis, ML Deck & CT Motion.	8.19	0.2	8.22	0.1	89	0.5	**8.21**	8.19	-0.2	8.22	0.2	**0.2**	0.1	-20	0.2	20	
ML Tower 3rd Lateral Bending Z-Axis, CSFSU Translation Y-Axis, VSS Motion, ML Deck Motion, CT 1st Bending Z-Axis & Translation X-Axis & Rotation About Y-Axis.	12.81	0.1	12.82	0.1	98	0.0	**12.81**	12.81	0.0	12.82	0.0	**0.1**	0.1	-18	0.1	18	**Harmonic**
CAA Translation X-Axis, ICPSU & CSFSU Translation Z-Axis In-Phase With Each Other, VSS Motion, ML Deck Motion, CT 1st Bending Z-Axis & Translation X-Axis & Rotation About Y-Axis.	14.07	0.0	14.06	0.0	98	-0.1	**14.06**	14.06	0.0	14.07	0.0	**0.0**	0.0	580	0.0	-580	**Harmonic**

= High confidence in this modes actually existing (i.e. identified by all methods).
= Medium confidence in this modes actually existing (i.e. identified by all frequency domain techniques or SSI-UPCX and two other frequency domain
= Low confidence in this mode actually existing (i.e. only identified by two methods).
= Very low confidence in this mode actually existing (i.e. only identified by one method).

Figure 29. CT Stopped Final Mode Set (normalized to lowest frequency File04 mode).

Figure 30 shows the MAC of the CT stopped final mode set. This shows relatively good separation of the modes, excluding the two harmonics. When a TAM becomes available, an ORTHO of the CT stopped final mode set should be computed to verify separation of these modes.

			1	2	3	4	5	6	7	8
			1.00	1.20	3.50	4.48	6.86	8.23	12.86	14.11
100	1	1.00	100			6				
95	2	1.20		100						
90	3	3.50			100					
85	4	4.48	6			100	5			
80	5	6.86				5	100			
75	6	8.23						100		12
70	7	12.86							100	
65	8	14.11						12		100

Figure 30. MAC CT Stopped Final Mode Set (modal frequencies normalized to 1st mode).

Figure 31 shows the XMAC of the CT stopped vs CT moving final mode sets, which shows that these modes were fundamentally different. Figure 32 shows the XMAC computed that excludes the test DOF on the CAA, umbilicals, and VSS, which results in the XMAC values for the first three modes to increase to 100% indicating these mode shapes are now essentially identical. Therefore the differences in the mode shapes of these first three modes (i.e., ML Tower 1st lateral bending Z-Axis, Y-Axis, and ML Tower 1st torsion) when the was CT stopped and CT moving are due to differences in the relative motions of the CAA, Umbilicals, and VSS indicating they have nonlinear characteristics. Because the XMAC values did not significantly improve for the remaining modes, this indicates differences in these mode shapes may be due to nonlinear characteristics in the ML and/or CT, or the three Engine Service Platforms (ESP's) residing below the flame hole that may be acting as a large tuned mass damper, which unfortunately were not instrumented.

			1	2	3	4	5	6	7	8	9	10	11	12	13	14	15	16	17
			1.00	1.16	3.53	4.74	6.12	7.95	8.98	9.60	9.70	10.53	10.58	11.70	13.26	13.60	14.58	15.37	15.42
100	1	1.02	34																
95	2	1.23		36															
90	3	3.58			75														
85	4	4.58				41													
80	5	7.02																	
75	6	8.42						50											
70	7	13.16																	
65	8	14.44														26			

Figure 31. XMAC of Final Mode Sets: CT Stopped (rows), CT Moving (columns) (modal frequencies normalized to lowest frequency mode).

			1	2	3	4	5	6	7	8	9	10	11	12	13	14	15	16	17
			1.00	1.16	3.53	4.74	6.12	7.95	8.98	9.60	9.70	10.53	10.58	11.70	13.26	13.60	14.58	15.37	15.42
100	1	1.02	100																
95	2	1.23		100															
90	3	3.58			100			48						27					
85	4	4.58				64	44												
80	5	7.02				22	22												
75	6	8.42			36			41						28					
70	7	13.16														41			
65	8	14.44																	

Figure 32. XMAC of Final Mode Sets Excluding Test DOF ON CAA, Umbilicals, VSS: CT Stopped (rows), CT Moving (columns) (modal frequencies normalized to lowest frequency mode).

Initially it was thought that the E-Stops would introduce a strong "twang" into the ML on CT and therefore provide good excitation for the two lowest frequency fundamental modes (i.e., ML Tower 1st lateral bending Z-Axis, Y-Axis, ML Tower

1st Torsion, etc.). However, this was not the case. Both during the E-Stops and during normal rolling the motion of the ML on CT was dominated by the third lowest frequency fundamental mode (i.e., ML Tower 1st Torsion). This was due to the retracted and stowed CAA being a relatively large mass significantly offset laterally from the center line of the ML in the fore-aft direction of travel (Z-Axis) so that any fore-aft motion of the ML Tower immediately caused the ML Tower to twist about the vertical (X-Axis) axis (i.e., torsion motion). This explains why the three automatically selected Projection Channels had not included any accelerometers in the fore-aft direction of travel (Z-Axis), but instead had two accelerometers in the lateral direction (Y-Axis) that well captured the torsion motion of the ML Tower.

Time histories of the CT accelerometers adjacent to the CT pickup points in each corner of the CT were compared to the time histories of the adjacent ML accelerometers during the first E-Stop. This comparison showed there was no vertical or lateral relative motion across the CT pickup points during the event that produced the highest lateral loads on the CT and therefore confirmed the assumption that the lateral mechanical constraints and friction forces were constraining relative motion in all lateral directions during the entire ISVV-010 rollout.

Figure 33 shows the File05 individual CT JEL oil pressures and the overall mean JEL pressure. The JEL pressures at CT Corners C & D were higher than those at CT Corners A & B because the CT pickup points at Corners A&B were closer to the ML center of gravity (cg). CT pickup points at Corners C & D are located under the ML Tower while the CT pickup points at CT Corners A&B are located out in front of the ML Tower. While the mean JEL pressure remains essentially constant, the individual JEL pressures were constantly changing, which was flexing the ML Deck and producing vibrations throughout the ML and CT. Furthermore, the JEL pressure changes were such that the highest loadings were constantly swapping between diagonally opposite corners of the CT (i.e., higher JEL pressures at CT Corners A and C swap with higher JEL pressures at CT Corners B and D).

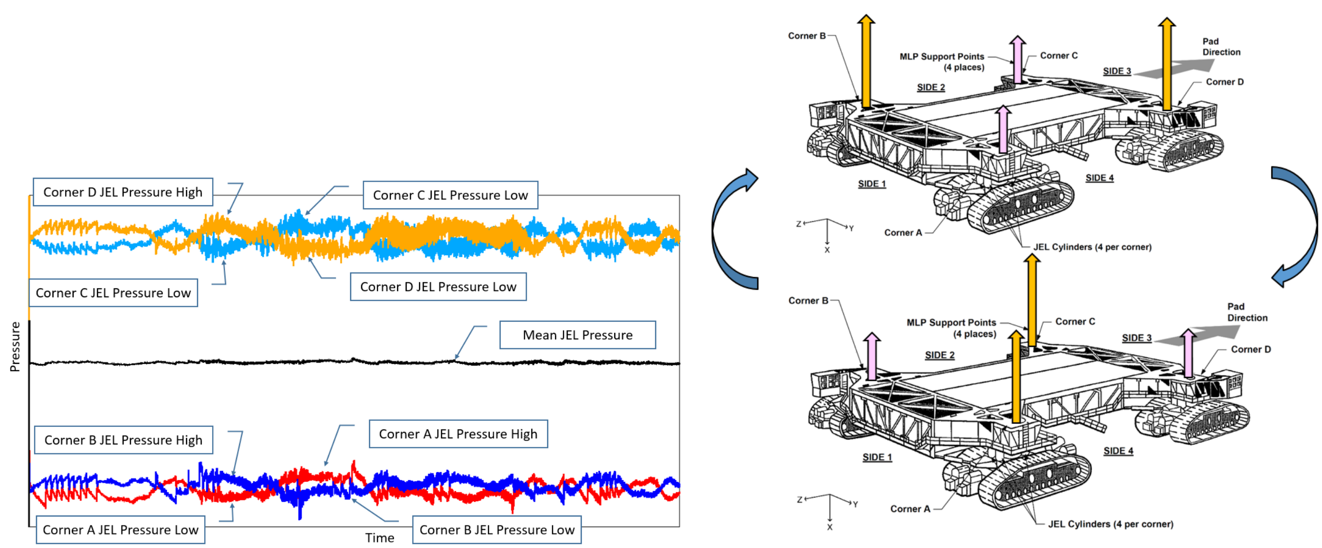

Figure 33. File05 JEL Pressure Time Histories: Corner A (red), Corner B (blue), Corner C (light blue), Corner D (orange), Mean (black).

Conclusions

OMA techniques will not replace traditional modal testing (i.e., Experimental Modal Analysis (EMA)), but can provide important supplemental information and insights into the structural dynamics of hardware in its operational environment. OMA techniques were successfully applied to the ISVV-010 rollout data for identifying fundamental ML on CT modes, important CT harmonics, and nonlinear characteristics of the ML on CT. These ML on CT nonlinear characteristics had not been identified during the ML modal test that immediately preceded the ISVV-010 rollout and were dependent upon whether the CT was moving or stopped, and upon the ground winds speed. This analysis showed during the rollout of the ML on CT for time intervals where the CT speed was constantly varying, but not varying too drastically (i.e., during an E-Stop), there was no need to perform time consuming and computer intensive harmonic reduction analysis to remove (or at least greatly reduce) the CT shoe and roller crossing harmonics before fundamental modes could be identified unlike with the rollouts of the CT or MLP on CT. OMA techniques were able to identify the highest number of modes from the File05 data set, which had a "stair step" pattern CT speed profile and the greatest overall variation in the CT speed while the CT was moving. OMA techniques were able to identify a higher number of modes when the CT was moving than when the CT was stopped. Fifteen fundamental ML on CT modes were identified when the CT was moving, but only six were identified when the CT was stopped. Having a TAM and a Target Mode set would have greatly aided in identifying the fundamental modes using OMA techniques, and may have led to a greater number of fundamental modes being identified for both CT operational regimes (i.e., moving and stopped). Based upon the ISVV-010 CT speeds, a one hour long CT speed profile has been developed that would aid OMA techniques in identifying the fundamental ML on CT modes if implemented during future ML on CT rollouts.

This analysis seems to indicate that a varying CT speed appears to "average out" the effects of the CT shoe and roller crossing harmonics, or at least greatly reduces them, leaving the ML on CT modes as the dominant response. However after this analysis was completed, the 2005 Shuttle-Era CT transporting the MLP rollout data and 2017 CT transporting the MLP rollout data was analyzed during periods where the CT speed was varying, which showed the CT shoe and roller crossing harmonics do not "average out" when the CT speed varies. Instead the analysis of the 2005 and 2017 rollout data indicates it was the additional mass loading of the ML and the broadband excitation produced by the ground winds impinging on the ML Tower are what allowed OMA techniques to identify the fundamental ML on CT modes without the need for first performing harmonic reduction analysis.

This analysis of the ISVV-010 rollout data has provided invaluable insights into the ML on CT dynamic characteristics. It showed the acceleration response levels on the ML Deck during the ISVV-010 rollout were significantly less than those on the ML Tower or CT, which is due to the known relatively weak structural coupling between the ML Tower and ML Deck and the relatively high mass of the ML Deck. This analysis of the ISVV-010 rollout data has also provided invaluable insights into what to expect during the upcoming rollout of the Artemis I flight vehicle where OMA techniques will be applied to the Artemis I rollout data to identify its fundamental modes. The analysis of the Artemis I rollout data and identification of its fundamental modes using OMA techniques will lead to better understanding the rollout dynamics, assist in correlating the ML and SLS FEM's, and assist in refining the rollout forcing functions. However, it is anticipated that using OMA techniques to identify the fundamental Artemis I rollout modes may be more challenging. There will be strong coupling of the Artemis I flight vehicle and ML on CT dynamics via the umbilicals and Vehicle Stabilizer System (VSS) that connects them and their known nonlinear characteristics, particularly the VSS. Also the additional mass of Artemis I (3.6 million pounds) and the high damping of the SLS boosters will further reduce the acceleration response levels on the ML Deck. If there are significant ground winds during the Artemis I rollout, the resulting broadband excitation of Artemis I and the ML Tower may help to offset the above detrimental effects and assist the OMA techniques in identifying the fundamental Artemis I rollout modes.

ACKNOWLEDGEMENTS
The authors would like to thank the NASA Engineering Safety Center (NESC) for funding this work and Professor Carlos Ventura of the University of British Columbia [20, 21] for his mentoring and guidance.

REFERENCES

[1] "SLS Fact Sheet.", https://www.nasa.gov/exploration/systems/sls/factsheets.html.

[2] "NASA Facts: Space Launch System.", https://www.nasa.gov/sites/default/ files/files/SLS-Fact-Sheet_aug2014-finalv3.pdf.

[3] "Mobile Launcher, NASA Fact Sheet." https://www.nasa.gov/sites/default/files/ atoms/files/mobilelauncher_ factsheet_v2.pdf.

[4] "Mobile Launcher Umbilicals and Support, NASA Facts." https://www.nasa.gov/sites/default/files/atoms/files/ ml_umbilicals20160523.pdf.

[5] Crawler-Transporters, NASA Fact Sheet.", https://www.nasa.gov/sites/default/files/638823main_crawler-transporter.pdf.
[6] "Crawler-Transporter 2, NASA Fact Sheet." https://www.nasa.gov/sites/default/files/atoms/files/crawler-transporter2_factsheet_508compliant.pdf.
[7] "Crawler-transporter", https://en.wikipedia.org/wiki/Crawler-transporter.
[8] James, G., Grady, R. Allen, M., Bruno, E., "Forcing Function Estimation for Space System Rollout." *Proceedings of the 39th International Modal Analysis conference*, 2020.
[9] Akers, J., Sills, J., "Space Launch System Mobile Launcher Modal Pretest Analysis.", *Proceedings of the 39th International Modal Analysis conference*, 2020.
[10] Stasiunas, E., Parks, R., Sontag, B., Chandler, D., "Modal Test of the NASA Mobile Launcher at Kennedy Space Center." *Proceedings of the 39th International Modal Analysis conference*, 2020.
[11] Sills, J. and Allen, M., "Historical Review of 'Building Block Approach' in Validation for Human Space Flight." *Proceedings of the 37th International Modal Analysis Conference*, 2019.
[12] "Mobile Launch Platforms (MLP)." https://science.ksc.nasa.gov/facilities/mlp.html.
[13] "Mobile launcher platform." https://en.wikipedia.org/wiki/Mobile_launcher_platform.
[14] "NASA - Behind the Rollout". https://www.nasa.gov/mission_pages/shuttle/flyout/rollout.html.
[15] Elliot, K., James, G., Buehrle, R., Richart, J., "Space Shuttle Transportation (Roll-Out) Loads Diagnostics." *Proceedings of the 23rd International Modal analysis Conference,* 2005
[16] Meyer, K., Nerolich, S., Burton, R., Gosselin, A., "Space Shuttle Crawler Transporter Vibration Analysis in Support of Rollout Fatigue Load Spectra Verification Program." *Proceedings of the 11th International Conference on Sound and Vibration,* 2004.
[17] Buehrle, R., Kappus, K., "Operating Deflection Shapes for the Space Shuttle Partial Stack Rollout." *Proceedings of the 23rd International Modal analysis Conference,* 2005.
[18] Winkel J., Akers J., and Bruno E., "Feasibility Study of SDAS Instrumentation's Ability to Capture Mobile Launcher/Crawler-Transporter Target Modes During Rollout Operations.", *Proceedings of the 38th International Modal Analysis Conference*, 2020.
[19] NASA-STD-5002*: Load Analyses Of Spacecraft And Payloads*, Section 4.2.6 f, June 21, 1996.
[20] Brinker, R., Ventura, C., *Introduction to OPERATIONAL MODAL ANALYSIS*, Wiley, New York, 2015.
[21] Andersen, P., Ventura, C., "Operational Modal Analysis: Background, Theory & Practice.", *39th International Modal Analysis conference preconference course*, 2020.